











Coagulation/flocculation for effective removal of green bromocresol using NP/Fe₃O₄: A statistical optimization approach for sustainable wastewater treatment

Mariam Attouch¹, Otman Goudali², Badreddine Hatimi¹, Asmae Sanad¹,
Meryem Bensemlali¹, Meryeme Joudi^{1,2}, Abdellatif Aarfane^{1,3},
Najoua Labjar⁴, Mina Bakasse¹, Hamid Nasrellah^{1,3}

¹ Laboratory of Organic Bioorganic Chemistry and Environment, Faculty of Sciences, University Chouaib Doukkali, El Jadida, Morocco

² Laboratory of Chemistry of Coordination and Analytics, Faculty of Sciences, B.P. 24000, El Jadida, Morocco

³ Higher School of Education and Training, University Chouaib Doukkali, El Jadida, Morocco

⁴ Laboratory of Spectroscopy, Molecular Modelling, Materials, Nanomaterials, Water and Environment, ENSAM, Mohammed V University in Rabat, Morocco

* Corresponding author's e-mail: nasrellah.h@ucd.ac.ma

ABSTRACT

Natural phosphate/Fe₃O₄ (NP/Fe₃O₄) was prepared by modifying natural phosphate with ferric chloride (FeCl₃). The resulting composite was characterized using Fourier transform infrared spectroscopy (FTIR) to identify functional groups and X-ray diffraction (XRD) to analyze its crystalline structure. A Box-Behnken design model was used to optimize three operational parameters: the initial pH, the dosage of NP/Fe₃O₄, and the initial concentration of green bromocresol (GBC), aiming to achieve maximum GBC removal from wastewater. Experimental tests were carried out using a six-beaker jar test setup to replicate the treatment process under controlled conditions. The findings revealed that GBC removal efficiency peaked at 97% when the pH was maintained between 4 and 7. This high efficiency demonstrates the effectiveness of NP/Fe₃O₄ as an adsorbent for wastewater treatment. Additionally, the study emphasized the crucial role of statistical optimization techniques in enhancing the removal of pollutants and improving the overall efficiency of treatment processes.

Keywords: natural phosphate/Fe₃O₄, green bromocresol, coagulation/flocculation, wastewater treatment, response surface methodology.

INTRODUCTION

Bromocresol green, one of the most widely used water soluble pH indicators, has shown to be particularly hazardous due to its stability in aquatic ecosystems (Rosa et al., 2019; Dehghani et al., 2016). Because this dye is not readily biodegradable, it can accumulate and create a potential hazard for water organisms by inhibiting biological processes in them or reducing their biodiversity. Humans may notice skin or eye irritation if large quantities of bromocresol green are directly and improperly handled. This made

it necessary to adequately treat and manage the wastewater containing these dyes, because of their toxic & hazardous nature towards animals including humans (Ahmed et al., 2024, Owino et al., 2023). Şenol et al. (2024), adsorption (Perez-Calderon et al., 2023), chemical treatments (Bustos-Terrones et al., 2021), advanced oxidation processes (Zhou et al., 2024) as well as coagulation and flocculation (Cheng et al., 2018; Muniasamy et al., 2023; Ihaddaden et al., 2022; Beluci et al., 2019).

Phosphates provide multiple advantages, especially in terms of stability and their applications

in various materials (Carvalho et al., 2023; Tang et al., 2023; Chauhan et al., 2024). Apart from the stability and wide utility in many materials, natural phosphate offers an array of advantages due to the porous structure and chemical properties of natural phosphates, they are utilized as efficient materials for removing dyes from wastewater (Hidayat et al., 2024; Liu et al., 2021; Zhang et al., 2022).

A property of phosphate-based materials is that the in-situ substitution of iron can render them magnetic, catalytic or modified structures depending on the composition and reaction conditions. (Padayachee et al., 2017). In addition, the phosphate-FeCl₃ composite might be suitable for use as a photocatalyst that is able to take advantage of solar energy in photochemical reactions for production of clean fuels and chemicals or environmental applications (Largo et al., 2024). In this study, the phosphate/Fe₃O₄ was used in the coagulation/flocculation process.

introducing diluted sodium hydroxide (CAS No: 1310-73-2; Sigma-Aldrich) or weak nitric acid (CAS No: 7697-37-2; VWR Chemicals), in order to achieve the needed pH using a Hanna Instruments pH meter. The distilled water employed in the present study was of first quality.

Preparation of NP/Fe₃O₄

The NP/ Fe₃O₄ was prepared from natural phosphate mixed with FeCl₃·6H₂O; 5 g of treated natural phosphate was blended with 10 mL of FeCl₃·6H₂O (100 g/L), the mixture was stirred continuously during 24 h. Then, it was followed by centrifugation using BIOBASE centrifuge and it was washed using distilled water to neutral pH. Afterward, the mixture was dried for 48 hours at 60 °C and it was calcined at 600 °C over 2 hours. The calcined product was finely ground in a mortar and sieved to obtain granular particles as shown in Figure 2.

MATERIALS AND METHODS

Materials

The ferric chloride hexahydrate (FeCl₃·6H₂O) employed in this study was used as received without any further treatment; this product was purchased from Sigma-Aldrich. Bromocresol green (CAS NO.:76-60-8) was obtained from OXFORD Lab and its chemical structure is presented in Figure 1. The natural phosphate used in this study was supplied from Khouribga, Morocco and was processed mainly by initial crushing. These steps involved grinding, washing and drying at 900 °C. Drying was performed in a Furnace brand oven, whereas sieving with a Biobase brand sieve within a particle size range of 100–400 μm. The pH of the solution was adjusted by

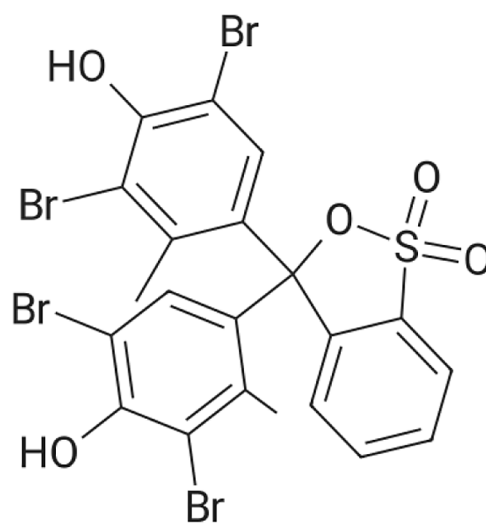


Figure 1. Structure of green bromocresol

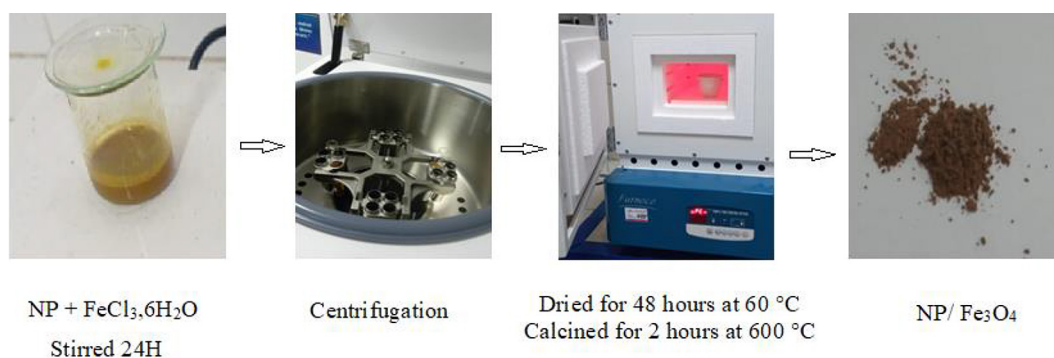


Figure 2. Preparation of NP/ Fe₃O₄ from natural phosphate

Apparatus and physicochemical techniques

X-ray powder diffraction (XRD) patterns were recorded on a PAN analytical XPert ProX instrument (Malvern Panalytical Ltd., Royston, UK). The instrument was performed under a Ni-filter condition with CuK α radiation ($\lambda = 1.54060 \text{ \AA}$) using an accelerating voltage V of 40 kV, and generated a current I of 30 mA. Data collection was carried out in scan range 5–70° (2 θ).

The surface chemical groups of the NP/Fe₃O₄ were analyzed by FTIR (nicolet 380 fourier transform infrared spectrometer) in the attenuated total reflectance (ATR) mode. The spectra were then collected in the range of 4000 to 600 cm⁻¹ with a 4 cm⁻¹ resolution.

Experimental procedure

Figure 3 shows the coagulation/flocculation process studied using a six-beaker jar test at different pH levels with a VELP Scientifica JLT6 Flocculation Tester. In each beaker 250 ml of dye solution was present. The process started with 2 min high-speed mixing on 100 rpm, followed by 15 minutes gentle mixing on 40 rpm and finished after another 10 min sedimentation. After settling phase, it was filtered using a 0.45 μm filter. The concentration of the dyes in the solutions was evaluated using a Jasco 660 UV-vis spectrophotometer at a wavelength of 615 nm. The dye removal percentage was calculated with the following Equation:

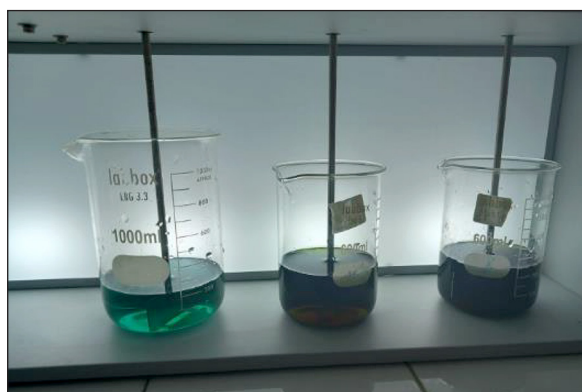


Figure 3. Coagulation/flocculation process test

$$\text{Dye removal (\%)} = \left(\frac{C_i - C_t}{C_i} \times 100 \right) \quad (1)$$

where: C_i and C_t represent the initial dye concentration and at time, respectively.

Experimental design and data analysis

The response surface methodology (RSM) was used to study the impact of influent factors, because it is considered as a robust statistical technique that maximizes global efficiency on the experimental plane (Sarah et al., 2023). The Box-Behnken design is a one of the numerous designs for RSM and often considered since it also requires fewer experiments to obtain predictable outcomes (Mokhtar et al., 2024; Alrefaee et al., 2024; El Gaayda et al., 2024). The Box-Behnken design was employed in this study using three levels: low (-) and high (+). The values for the factors are summarized in Table 1.

Regression model equation

$$Y = \beta_0 + \sum_{i=1}^k \beta_i X_i + \sum_{i=1}^k \beta_{ii} X_i^2 + \sum_{i < j}^k \beta_{ij} X_i X_j + \epsilon \quad (2)$$

where: Y is the response variable, β_0 is the intercept, β_i are the linear coefficients, β_{ii} are the quadratic coefficients, and β_{ij} represent the interaction coefficients.

The independent variables are denoted by X_i and X_j , and ϵ is the error term (El Gaayda et al., 2024).

ANOVA F-ratio

The F-ratio in ANOVA is a statistical value used to assess whether the means of different groups are significantly different from each other. It is computed by comparing the variance between the groups to the variance within each group, helping to evaluate the effect of the independent variable. A larger F-ratio suggests a higher probability that the differences observed between groups are not due to random variability

Table 1. Values of three factors

Description	Factor	Unit	-1	+1
pH solution	X_1	UpH	4	10
Initial GBC concentration	X_2	mg/L	10	100
NP/Fe ₃ O ₄ dosage	X_3	g/L	0.1	0.55

(O’Driscoll et al., 2024; Rodrigues et al., 2024; Chen et al., 2021).

$$F = \frac{\text{Mean square of factor}}{\text{Mean square of error}} \quad (3)$$

This is used to test the significance of factors in the model.

RESULTS AND DISCUSSION

DRX analysis

Figure 4 shows the X-ray diffraction (XRD) pattern of both the NP and the synthesized NP/Fe₃O₄ samples. The analysis revealed distinct peaks at 2θ angles of 25,09°, 31,8°, 32,2°, and 32,9°, which are characteristic of NP. These diffraction peaks correspond to the specific crystallographic planes (002), (211), (112), and (300) of the NP phase. The characteristic Fe₃O₄ peaks are typically found closer to 30° and 35,29° for the (220) and (311) planes

confirming the successful incorporation of iron oxide into NP (Patwa et al., 2024; Fu et al., 2020).

FTIR analysis

Figure 5 shows the FTIR of NP and NP/Fe₃O₄. NP was characterized using FTIR, to identify all functional groups present in Fe₃O₄ (Joudi et al., 2019). The band observed at 864 cm⁻¹ was assigned to Si-O bending vibrations due to the silicate groups present in NP (Naciri et al., 2016). The band detected at 1100 cm⁻¹ was assigned to P-O stretching vibrations (Gungor Koc, 2019). The carbonate ions were detected within the 1360–1400 cm⁻¹ region, and attributed to CO₃²⁻ bending vibrations (Dakkach et al., 2012). The band at 2400 cm⁻¹ confirmed the existence of CO (Lalliansanga et al., 2022). The bands showed at 2800 cm⁻¹ represented C-H stretching vibration, indicating the presence of hydrocarbon

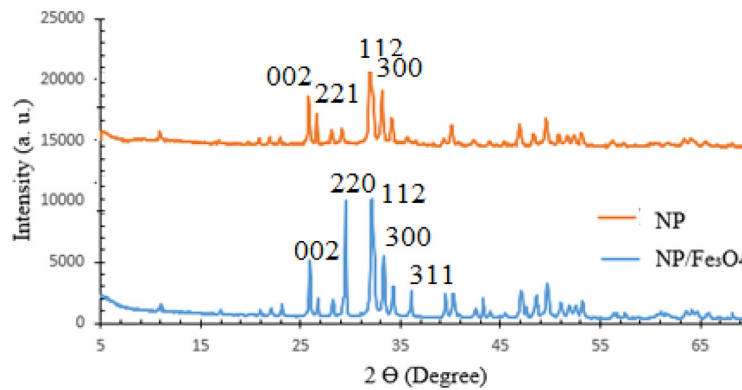


Figure 4. XRD of NP and NP/Fe₃O₄

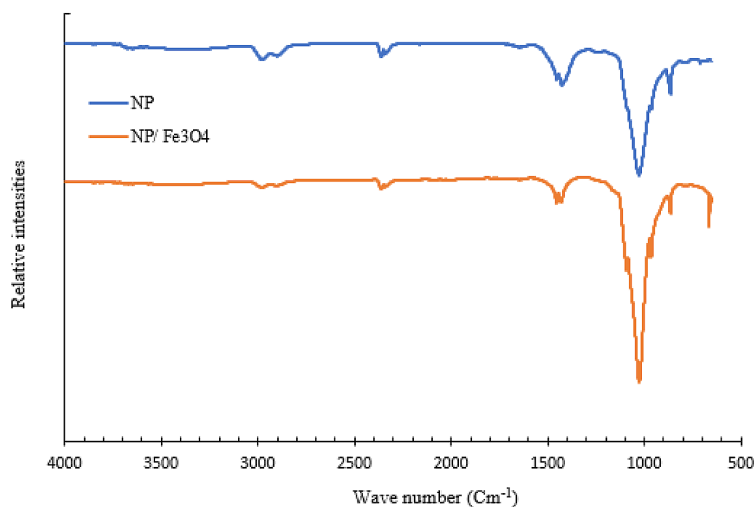


Figure 5. FTIR of NP and NP/Fe₃O₄

(Wacharine et al., 2024; Zhu et al., 2014; Nasef et al., 2019). Similarly, all those characteristic bands found in the NP sample were also detected from the FTIR spectra of NP/Fe₃O₄ composite indicating a proper preparation of NP/Fe₃O₄. The band at 1100 cm⁻¹ was associated to the O-H stretching vibrations, therefore showing that OH groups were present in the product. A novel band at 640 cm⁻¹ was detected, which exhibited Fe-O stretching vibrations in magnetite (Wacharine et al., 2024).

The pH point zero charge (PZC)

Point of zero charge (PZC) represents pH when the surface charge is neutral; i.e. there are equal positive as well as negative charges present on a material surface. This is an important point, as it decides how the material interacts with ions in a solution (Obeid et al., 2013).

A 0.1 mol·L⁻¹ NaCl solution (Fulka) with a pH range between 2 and 12, adjusted by adding an aqueous solution of NaOH or HCl, was first prepared. Then, 0.1 g of dried NP/Fe₃O₄ was brought into contact with 20 mL of each solution in sealed flasks. The suspensions were stirred for three days at room temperature using a Reciprocating Shaker RSLAB-7 at a constant speed. After agitation, each solution was filtered through a 0.45 μm cellulose filter paper, and the pH was measured again. Figure 6 illustrates the pH PZC tests of NP/Fe₃O₄. In Figure 7, the change in ΔpH corresponding to the variation in initial pH is reported. ΔpH=0 represents the pH point of zero charge (pHpzc) and this is evident from Figure 7 at around initial

pH of near about 7. Thus, at pH 7, the material is uncharged on average.

In the pH range of less than 7, ΔpH is negative, which indicates that the material releases H⁺ ions into solution and confers a positive surface charge under acidic conditions. In contrast, when the pH further increased to above 7 the value of ΔpH changed into positive meaning that the material absorbs protons (H⁺) and therefore carrying a surface negative charge as in basic medium.

Development of regression model equation and validation of the model

The Box-Behnken design was employed to investigate the impact of three factors: pH, green bromocresol (GBC) concentration, and coagulant



Figure 6. Determination of the pH point zero charge

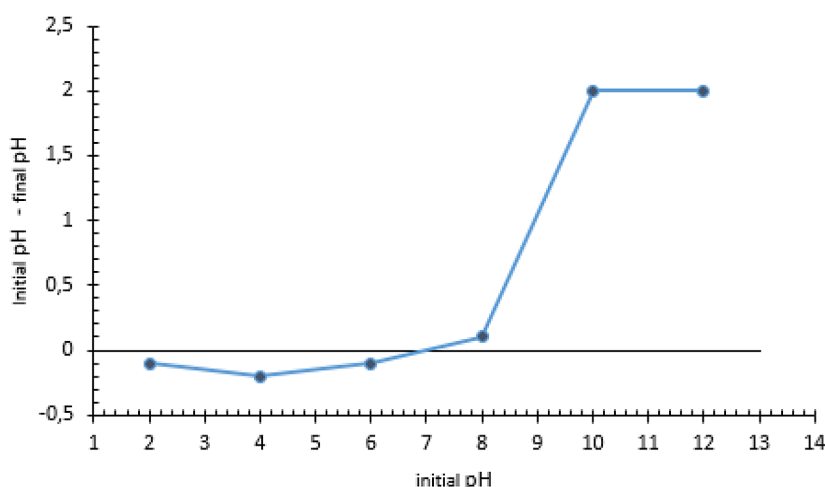


Figure 7. Effect of initial solution pH on ΔpH as a function of pH before and after adjustment for the Fe₃O₄/natural phosphate composite

Table 2. Box-Behnken design for GBC dye removal

N°	Configuration	pH	GBC concentration (mg/L)	NP/Fe ₃ O ₄ Dose (g/L)	Removal of GBC %
1	000	7	55	0.55	100
2	-0+	4	55	1	98
3	0+-	7	100	0.1	99
4	0++	7	100	1	97
5	++0	10	100	0.55	2
6	-+0	4	100	0.55	100
7	000	7	55	0.55	98
8	0--	7	10	0.1	99
9	000	7	55	0.55	97
10	0-+	7	10	1	97
11	+0-	10	55	0.1	4
12	-0-	4	55	0.1	96
13	--0	4	10	0.55	96
14	+0+	10	55	1	3
15	+0-	10	10	0.55	5

dosage, on the coagulation/flocculation process. The percentage of dye removal was considered as the response variable in the study. Table 2 provides a detailed overview of the experimental results for these factors. This design was chosen for its efficiency in exploring interactions between variables while minimizing the number of experimental runs based in a second-order polynomial model with interaction terms created by JMP Pro 13.

The estimated coefficients in the model, and the t Ratio, and Probability values for all linear, quadratic, and interaction effects of the parameters, are summarized in Table 3. The t ratio and probability were used to evaluate a regression model. A higher t ratio combined to lower probability to suggest that the factor is significant. Figure 8 illustrates the Pareto chart analysis and

the bar length shown in this chart corresponds to the impact of each factor. It was observed that the most significant factor in this study was the pH. Table 4 presents the analysis of variance (ANOVA) results for a model. This table shows that the model explains a significant portion of the variability, with a sum of squares of 24,134.32 and a mean square of 2,681.59, compared to the error with a sum of squares of 85.42. The F-ratio of 156.97 is very high, and the corresponding P-value (<0.0001) indicates that the probability of observing such a result by chance (Prob > F) is extremely low. This confirms that the model is statistically significant, denoted by the (*) under the significance column [19].

In Figure 9, the plot demonstrates a strong linear relationship between the predicted and actual

Table 3. Estimated regression coefficient for % removal of GBC

Term	Estimate	Std error	t Ratio	Prob> t
Intercept	98.3333	2.3863	41.2100	<.0001
pH (4.10)	-43.1250	1.4613	-29.5100	<.0001
GBC concentration (mg/L) (10.100)	-5.5000	1.4613	-3.7600	0.0131
NP/Fe ₃ O ₄ dose (g/L) (0.1.1)	6.1250	1.4613	4.1900	0.0086
pH*GBC concentration (mg/L)	1.2500	2.0666	0.6000	0.5717
pH*NP/Fe ₃ O ₄ dose (g/L)	-5.5000	2.0666	-2.6600	0.0448
GBC concentration (mg/L)*NP/Fe ₃ O ₄ dose (g/L)	8.2500	2.0666	3.9900	0.0104
pH*pH	-47.4167	2.1510	-22.0400	<.0001
GBC concentration (mg/L)*GBC concentration (mg/L)	-3.1667	2.1510	-1.4700	0.2009
NP/Fe ₃ O ₄ dose (g/L)*NP/Fe ₃ O ₄ dose (g/L)	-5.4167	2.1510	-2.5200	0.0533

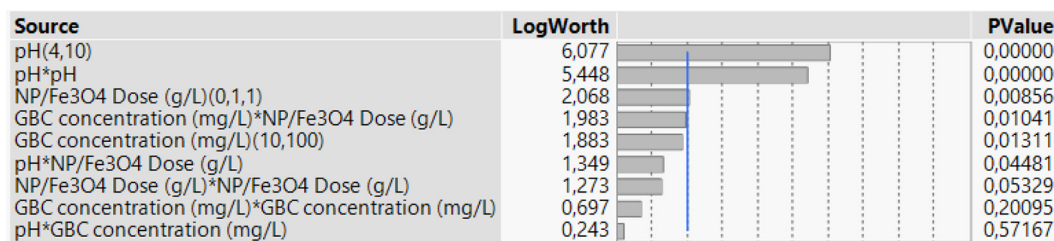


Figure 8. Pareto chart analysis for removal of GBC

Table 4. Analysis of variance (ANOVA) for the removal of GBC

Source	Degree of freedom	Sum of squares	Mean square	F ratio	P-Value	Significance
Model	9	24 134.32	2 681.59	156.97	<0.0001	*
Error	5	85.42	17.08	–	–	–
Total	14	24 219.73	–	–	–	–

Note: * Significant at a level of 5% (F0.050 (1, 15) = 4.54).

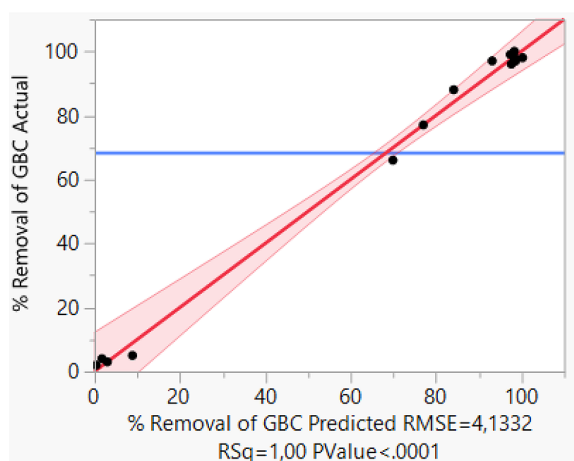


Figure 9. The graph depicting the relationship between the predicted and actual values for GBC removal

percentages of GBC removal. The high R-squared value of 1.00 indicates excellent agreement between the two, while the low RMSE (4.1332) and significant P-value (<0.0001) highlight the accuracy and reliability of the model. The equation of the removal of GBC as a function of the selected factors is expressed as follows:

$$\begin{aligned}
 \text{GBC removal (\%)} = & 98.33 - 43.12(\text{pH}) - \\
 & - 5.5(\text{GBC concentration}) + 6.13(\text{NP/Fe}_3\text{O}_4 \text{ dose}) + \\
 & + 6.12 (\text{pH} \times \text{GBC concentration}) - \\
 & - 5.5(\text{pH} \times \text{NP/Fe}_3\text{O}_4 \text{ dose}) + \\
 & + 8.25(\text{GBC concentration} \times \text{NP/Fe}_3\text{O}_4 \text{ dose}) \quad (4)
 \end{aligned}$$

The negative coefficients for pH and GBC concentration suggest that higher values of these factors reduce removal efficiency, while an

increase in NP/Fe₃O₄ dose positively influences GBC removal. The interaction terms show that combinations of pH with GBC concentration or NP/Fe₃O₄ dose have a significant impact, and quadratic terms indicate diminishing returns at extreme values of the factors. Rsq=1 indicates that the calculated values were closely aligned with the experimental values, which suggests that this model was highly reliable for determination of %removal of GBC.

Figure 10 shows the influence of the pH, initial GBC dye concentration, and coagulant dose on both % removal of GBC dye and desirability. The optimal conditions of coagulation of GBM are achieved at pH 7, 61.23 mg/L of GBC concentration and 0.55 g/L of NP/Fe₃O₄ coagulant dose.

The desirability curve suggests that the maximum efficiency for GBC removal occurs when all three parameters are balanced at their optimal points, with a desirability score approaching 0.87, indicating a highly effective removal process under these conditions.

- Effect of pH: Figure 10 shows that as the pH increases from 4 to 10, the percentage of GBC removal initially increases, reaching a maximum around pH 7, and then decreases, which indicates that the optimal pH was less than or equal to 7.
- Effect of GBC concentration: Figure 10 indicates that increasing of GBC concentration results in a decrease in the % removal of GBC.
- Effect of NP/Fe₃O₄ dose: Figure 10 suggests that increasing the dose of NP/Fe₃O₄ up to 0.55 g/L positively impacts the % removal of GBC.

Figure 11 shows the 3D surface response for coagulation of GBC. This graphic was used to study the relationship between three key factors and % removal of GBC dye. The relationship between pH, initial GBC dye is shown in Figure 11a, it can be observed that the removal of GBC dye increases by decreasing initial dye concentration and keeping pH between 4 to 7. Figure 11b indicates that % removal of GBC increases with keeping the pH between 4 to 7. In turn, Figure 11c shows that % removal of GBC increases with decreasing initial dye concentration

Mechanism of coagulation of GBC using NP/Fe₃O₄

The coagulation of bromocresol green (GBC) dye using NP/Fe₃O₄ nanoparticles is based on electrostatic interactions. In the pH range of 4 to 7, GBC molecules, which carry a negative charge due to their functional groups, are attracted to the positively charged surface of the NP/Fe₃O₄ particles. This interaction promotes the aggregation

of dye molecules, facilitating their removal from the solution. The mechanism is validated by determining the point of zero charge (pH_{pzc}) of NP/Fe₃O₄, which confirms that the nanoparticles possess a positive surface charge under acidic to slightly neutral conditions. Furthermore, response surface analysis supports the influence of these charge interactions, demonstrating enhanced dye removal efficiency within the optimal pH range. This process demonstrates the capability of NP/Fe₃O₄ nanoparticles to act as an effective coagulant for anionic dyes, with their surface charge properties playing a key role in driving the coagulation mechanism.

Comparison of maximum removal of GBC with literature values

Table 5 shows the comparison in the literature regarding the determination of GBC. GBC removal has been studied using conventional coagulants and advanced materials. While traditional methods like aluminum

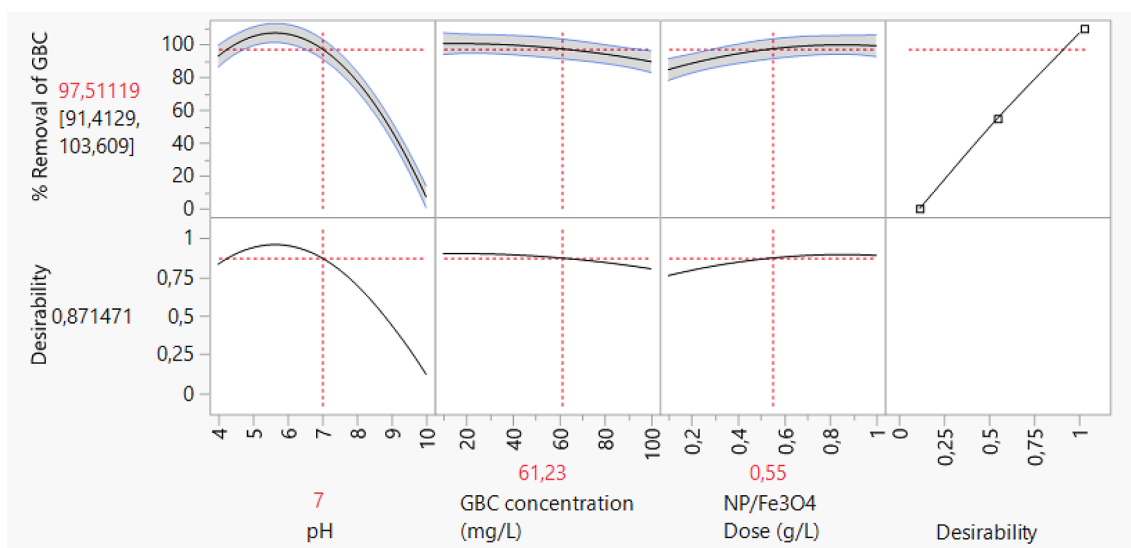



Figure 10. Main effects of parameters on the responses (desirability and % removal of GBC)

Table 5. Comparison of maximum removal efficiency of GBC with literature values

Materials	Illustration	Dose (g/L)	Removal of GBC (%)	References
NP/Fe ₃ O ₄		0.55	97.51%	This study
Acid functionalized corn cob	–	0.76	96%	(Onu et al., 2022)
Modified agricultural waste	–	20	93%	(Chijioke Elijah et al., 2020)

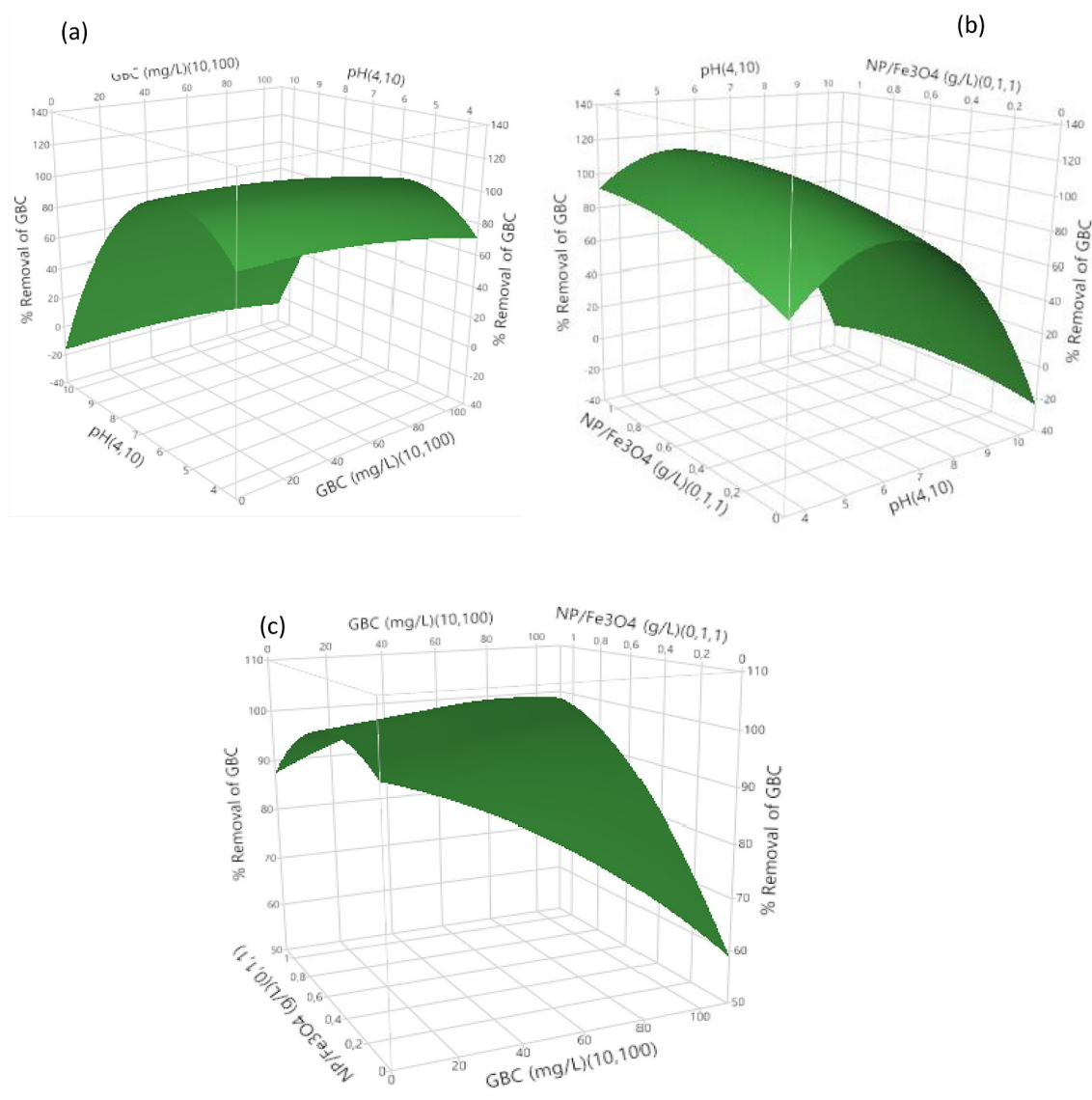


Figure 11. Response surface model of GBC removal (%) by three factors. Interaction between (a) initial concentration of GBC and pH, (b) pH and NP/Fe₃O₄ dose, (c) initial concentration of GBC and NP/Fe₃O₄ dose

salts produce excess sludge and have limited efficiency, Fe₃O₄ nanoparticles show superior performance through electrostatic interactions at pH levels below their p_{H_{pzc}}. These nanoparticles offer faster removal, higher selectivity, and easier recovery, making them a promising alternative for GBC wastewater treatment.

CONCLUSIONS

An efficient material has been developed from phosphate doped with FeCl₃ to enhance the coagulation of bromocresol green. The results from XRD and FITR show that NP/Fe₃O₄

was successfully prepared. In turn, the results from the response surface model demonstrate that NP/Fe₃O₄ effectively removes bromocresol green within a pH range of 4 to 7, showing a reduction in dye concentration as the dosage of the prepared material increases. The proposed mechanism confirms that the coagulation process was achieved by electrostatic interaction between negative charge of GBC and positive charge of the prepared coagulant. Moreover, the elimination of GBC using NP/Fe₃O₄ was highly effective, requiring only 0.55 g/L of the material, which compares favorably with other studies that generally require higher dosages for similar dye removal processes.

REFERENCES

- Ahmed, S., Sahoo, D., Brandão, P., Bhunia, S., Baran Manik, N., & Sinha, C. (2024). Carboxylate bridging Cd(II)-based 1D coordination polymer: Structure, fabrication of Schottky device and selective sorption of Bromocresol Green. *Inorganica Chimica Acta*, 572, 122277. <https://doi.org/10.1016/j.ica.2024.122277>
- Alrefaie, S. H., Aljohani, M. M., Alatawi, I. S. S., Sari, A. A. A., Alrashdi, K. S., Mogharbel, A. T., Alanazi, M. A. A., & El-Metwaly, N. M. (2024). Tailoring magnetic La-MOF for efficient Brilliant blue FCF dye removal using Box-Behnken design optimization. *Journal of Molecular Liquids*, 401, 124648. <https://doi.org/10.1016/j.molliq.2024.124648>
- Beluci, N. D. C. L., Mateus, G. A. P., Miyashiro, C. S., Homem, N. C., Gomes, R. G., Fagundes-Klen, M. R., Bergamasco, R., & Vieira, A. M. S. (2019). Hybrid treatment of coagulation/flocculation process followed by ultrafiltration in TiO₂-modified membranes to improve the removal of reactive black 5 dye. *Science of The Total Environment*, 664, 222–229. <https://doi.org/10.1016/j.scitotenv.2019.01.199>
- Bustos-Terrones, Y. A., Hermosillo-Nevárez, J. J., Ramírez-Pereda, B., Vaca, M., Rangel-Peraza, J. G., Bustos-Terrones, V., & Rojas-Valencia, M. N. (2021). Removal of BB9 textile dye by biological, physical, chemical, and electrochemical treatments. *Journal of the Taiwan Institute of Chemical Engineers*, 121, 29–37. <https://doi.org/10.1016/j.jtice.2021.03.041>
- Carvalho, T. S. S., Ribeiro, N., Torres, P. M. C., Almeida, J. C., H. Belo, J., Araújo, J. P., Ramos, A., Oliveira, M., & Olhero, S. M. (2023). Magnetic polylactic acid-calcium phosphate-based biocomposite as a potential biomaterial for tissue engineering applications. *Materials Chemistry and Physics*, 296, 127175. <https://doi.org/10.1016/j.matchemphys.2022.127175>
- Chauhan, T., Szöri-Dorogházi, E., Muránszky, G., Kecskés, K., Finšgar, M., Szabó, T., Leskó, M., Németh, Z., & Hernadi, K. (2024). Application of modified clays in the removal of phosphates and E. coli from aqueous solution. *Environmental Nanotechnology, Monitoring & Management*, 22, 100965. <https://doi.org/10.1016/j.enmm.2024.100965>
- Chen, W.-H., Chiu, G.-L., Chyuan Ong, H., Shiung Lam, S., Lim, S., Sik Ok, Y., & E.Kwon, E. (2021). Optimization and analysis of syngas production from methane and CO₂ via Taguchi approach, response surface methodology (RSM) and analysis of variance (ANOVA). *Fuel*, 296, 120642. <https://doi.org/10.1016/j.fuel.2021.120642>
- Cheng, Z., Yang, B., Chen, Q., Ji, W., & Shen, Z. (2018). Characteristics and difference of oxidation and coagulation mechanisms for the removal of organic compounds by quantum parameter analysis. *Chemical Engineering Journal*, 332, 351–360. <https://doi.org/10.1016/j.cej.2017.09.065>
- Chijioke Elijah, O., Nonso Collins, O., Callistus Obumneme, O., & Jessica, N.-B. (2020). Application of Modified Agricultural Waste in the Adsorption of Bromocresol Green Dye. *Asian Journal of Chemical Sciences*, 15–24. <https://doi.org/10.9734/ajocs/2020/v7i119011>
- Dakkach, M., Atlamsani, A., & Sebti, S. (2012). Le phosphate naturel modifié au vanadium: Un nouveau catalyseur pour l'oxydation des cycloalcanones et des α -cétols en présence de l'oxygène moléculaire. *Comptes Rendus. Chimie*, 15(6), 482–492. <https://doi.org/10.1016/j.crci.2012.03.003>
- Dehghani, M. H., Mahdavi, P., Tyagi, I., Agarwal, S., & Gupta, V. K. (2016). Investigating the toxicity of acid dyes from textile effluent under UV/ZnO process using *Daphnia magna*. *Desalination and Water Treatment*, 57(51), 24359–24367. <https://doi.org/10.1080/19443994.2016.1141327>
- El Gaayda, J., Titchou, F.-E., Karmal, I., Barra, I., Errami, M., Yap, P.-S., Oh, W.-D., Iqbal, A., Silanpää, M., Hamdani, M., & Akbour, R. A. (2024). Application of grape seed and *Austrocylindropuntia* mucilage for the simultaneous removal of azo dye and turbidity from synthetic wastewater: Optimizing experimental conditions using Box-Behnken Design (BBD). *Journal of Water Process Engineering*, 58, 104718. <https://doi.org/10.1016/j.jwpe.2023.104718>
- Fu, C.-C., Tran, H. N., Chen, X.-H., & Juang, R.-S. (2020). Preparation of polyaminated Fe₃O₄@chitosan core-shell magnetic nanoparticles for efficient adsorption of phosphate in aqueous solutions. *Journal of Industrial and Engineering Chemistry*, 83, 235–246. <https://doi.org/10.1016/j.jiec.2019.11.033>
- Gungor Koc, S. (2019). Synthesis and characterization of strontium and chlorine co-doped tricalcium phosphate. *Materials Letters*, 248, 69–72. <https://doi.org/10.1016/j.matlet.2019.03.136>
- Hidayat, E., Sarbani, N. M. M., Samitsu, S., Mitoma, Y., Aoyagi, M., Yonemura, S., & Harada, H. (2024). Porous sodium alginate/poly (acrylic acid) composites cross-linked with FeCl₃ for acid black 1 dye removal from aqueous solution. *Desalination and Water Treatment*, 319, 100407. <https://doi.org/10.1016/j.dwt.2024.100407>
- Ihaddaden, S., Aberkane, D., Boukerroui, A., & Robert, D. (2022). Removal of methylene blue (basic dye) by coagulation-flocculation with biomaterials (bentonite and *Opuntia ficus indica*). *Journal of Water Process Engineering*, 49, 102952. <https://doi.org/10.1016/j.jwpe.2022.102952>

17. Joudi, M., Hafdi, H., Mouldar, J., Nasrellah, H., Hatimi, B., El Mhammedi, M. A., & Bakasse, M. (2019). Removal of azodyes using natural phosphate doped by titanium dioxide (NP-TiO₂) nanoparticles. *Desalination and Water Treatment*, 168, 298–307. <https://doi.org/10.5004/dwt.2019.24399>
18. Lalliansanga, Tiwari, D., Tiwari, A., Shukla, A., Shim, M. J., & Lee, S.-M. (2022). Facile synthesis and characterization of Ag(NP)/TiO₂ nanocomposite: Photocatalytic efficiency of catalyst for oxidative removal of Alizarin Yellow. *Catalysis Today*, 388–389, 125–133. <https://doi.org/10.1016/j.cattod.2020.09.010>
19. Largo, F., Haounati, R., Ighnih, H., Malekshah, R. E., Rhaya, M., Ouachtak, H., El Hankari, S., Jada, A., & Addi, A. A. (2024). Effective removal of toxic dye from wastewater via advanced modified magnetic sepiolite using combined surfactants SDS/CTAB/Fe₃O₄@Sep: Empirical and computational analysis studies. *Journal of Molecular Liquids*, 407, 125114. <https://doi.org/10.1016/j.molliq.2024.125114>
20. Liu, J., Huang, L., Zou, H., Xie, W., Evrendilek, D. E., Luo, G., & Ninomiya, Y. (2021). Do FeCl₃ and FeCl₃/CaO conditioners change pyrolysis and incineration performances, emissions, and elemental fates of textile dyeing sludge? *Journal of Hazardous Materials*, 413, 125334. <https://doi.org/10.1016/j.jhazmat.2021.125334>
21. Mokhtar, A., Abdelkrim, S., Sardi, A., Hachemaoui, M., Chaibi, W., Chergui, F., Boukoussa, B., Djelad, A., Sassi, M., & Abboud, M. (2024). A strategy for the efficient removal of acidic and basic dyes in wastewater by organophilic magadiite@alginate beads: Box-Behnken Design optimization. *International Journal of Biological Macromolecules*, 277, 134348. <https://doi.org/10.1016/j.ijbiomac.2024.134348>
22. Muniasamy, S. K., AlObaid, A. A., Warad, I., & Ravindiran, G. (2023). Removal of brilliant green dye in aqueous solution using synthetic coagulation and flocculation technique. *Desalination and Water Treatment*, 314, 231–240. <https://doi.org/10.5004/dwt.2023.30093>
23. Naciri, N., Farahi, A., Rafqah, S., Nasrellah, H., El Mhammedi, M. A., Lançar, I., & Bakasse, M. (2016). Effective photocatalytic decolorization of indigo carmine dye in Moroccan natural phosphate–TiO₂ aqueous suspensions. *Optical Materials*, 52, 38–43. <https://doi.org/10.1016/j.optmat.2015.12.011>
24. Nasef, S., Badawy, N., Hafez, F., Slim, S., & El Nesr, E. (2019). Preparation and characterization of magnetic nanocomposite based on gum arabic/2-hydroxyethylmethacrylate using gamma irradiation for use in biomedical application. *Arab Journal of Nuclear Sciences and Applications*, 52(2), 209–226. <https://doi.org/10.21608/ajnsa.2019.4636.1106>
25. Obeid, L., Bée, A., Talbot, D., Jaafar, S. B., Dupuis, V., Abramson, S., Cabuil, V., & Welschbillig, M. (2013). Chitosan/maghemite composite: A mag-sorbent for the adsorption of methyl orange. *Journal of Colloid and Interface Science*, 410, 52–58. <https://doi.org/10.1016/j.jcis.2013.07.057>
26. O’Driscoll, C., Owodunni, O., & Asghar, U. (2024). Optimization of 3D printer settings for recycled PET filament using analysis of variance (ANOVA). *Helvion*, 10(5), e26777. <https://doi.org/10.1016/j.helivon.2024.e26777>
27. Onu, C. E., Ohale, P. E., Ekwueme, B. N., Obiora-Okafo, I. A., Okey-Onyesolu, C. F., Onu, C. P., Ezema, C. A., & Onu, O. O. (2022). Modeling, optimization, and adsorptive studies of bromocresol green dye removal using acid functionalized corn cob. *Cleaner Chemical Engineering*, 4, 100067. <https://doi.org/10.1016/j.clce.2022.100067>
28. Owino, E. K., Shikuku, V. O., Nyairo, W. N., Kowenje, C. O., & Otieno, B. (2023). Valorization of solid waste incinerator fly ash by geopolymer production for removal of anionic bromocresol green dye from water: Kinetics, isotherms and thermodynamics studies. *Sustainable Chemistry for the Environment*, 3, 100026. <https://doi.org/10.1016/j.scenv.2023.100026>
29. Padayachee, D., Dasireddy, V. D. B. C., Singh, S., Friedrich, H. B., Bharuth-Ram, K., & Govender, A. (2017). An investigation of iron modified hydroxyapatites used in the activation of n-octane. *Molecular Catalysis*, 438, 256–266. <https://doi.org/10.1016/j.mcat.2017.05.032>
30. Patwa, R., Rohilla, S., Saini, J., & Rani, U. (2024). Characterization of structural and spectroscopic properties of ZnO/Fe₂O₃ nanocomposites. *Ceramics International*, S027288422404046X. <https://doi.org/10.1016/j.ceramint.2024.09.078>
31. Perez-Calderon, J., Marin-Silva, D. A., Zaritzky, N., & Pinotti, A. (2023). Eco-friendly PVA-chitosan adsorbent films for the removal of azo dye Acid Orange 7: Physical cross-linking, adsorption process, and reuse of the material. *Advanced Industrial and Engineering Polymer Research*, 6(3), 239–254. <https://doi.org/10.1016/j.aiepr.2022.12.001>
32. Rodrigues, L. G. P., Coelho, F. R., Krummenauer, A., Nardelli, V. C., & França, F. H. R. (2024). Two-way ANOVA analysis of novel ALBDF functions obtained for H₂O CO₂ gas mixtures considering variable mole fraction ratios in oxy- and air-fuel combustion conditions. *Journal of Quantitative Spectroscopy and Radiative Transfer*, 320, 108973. <https://doi.org/10.1016/j.jqsrt.2024.108973>
33. Rosa, J. M., Garcia, V. S. G., Boiani, N. F., Melo, C. G., Pereira, M. C. C., & Borrelly, S. I. (2019). Toxicity and environmental impacts approached in the dyeing of polyamide, polyester and cotton knits. *Journal of Environmental Chemical Engineering*, 7(2),

102973. <https://doi.org/10.1016/j.jece.2019.102973>
34. Sarah, M., Misran, E., Maulina, S., & Madinah, I. (2023). Optimization of fermentation condition to produce liquid organic fertilizer (LOF) from rotten vegetable waste using response surface methodology. *Cleaner Engineering and Technology*, 16, 100679. <https://doi.org/10.1016/j.clet.2023.100679>
 35. Şenol, Z. M., El Messaoudi, N., Ciğeroglu, Z., Miyah, Y., Arslanoğlu, H., Bağlam, N., Kazan-Kaya, E. S., Kaur, P., & Georgin, J. (2024). Removal of food dyes using biological materials via adsorption: A review. *Food Chemistry*, 450, 139398. <https://doi.org/10.1016/j.foodchem.2024.139398>
 36. Tang, Y., Che, Y.-J., Bai, X.-Y., Wang, Z.-Y., & Gu, S.-Y. (2023). Effects of application of phosphate and phosphate-solubilizing bacteria on bacterial diversity and phosphorus fractions in a Phaeozems. *Heliyon*, 9(12), e22937. <https://doi.org/10.1016/j.heliyon.2023.e22937>
 37. Wacharine, C., Dridi, A., Ben Hassen, S., Nouri, F., Mosbah, A., Charradi, K., Trabelsi-Ayadi, M., & Ternane, R. (2024). Zinc doped calcium phosphate-sulfate hydroxyapatites: Synthesis, characterization, bioactivity, cytotoxicity and antibacterial properties. *Ceramics International*, S0272884224035764. <https://doi.org/10.1016/j.ceramint.2024.08.120>
 38. Zhang, R., Wen, K., & Han, R. (2022). Effective removal of phosphate from solution by iron-doped chitosan/polyvinyl alcohol composite membrane. *Desalination and Water Treatment*, 267, 98–107. <https://doi.org/10.5004/dwt.2022.28690>
 39. Zhou, B., Wang, J. J., Dangal, P., Lomnicki, S., Roy, A. D., & Park, J.-H. (2024). A novel sugarcane residue-derived bimetallic Fe/Mn-biochar composite for activation of peroxymonosulfate in advanced oxidation process removal of azo dye: Degradation behavior and mechanism. *Journal of Water Process Engineering*, 58, 104740. <https://doi.org/10.1016/j.jwpe.2023.104740>
 40. Zhu, C., Lu, Y., Chen, J., & Yu, S. (2014). Photo-thermal poly (*N*-isopropylacrylamide)/Fe₃O₄ nanocomposite hydrogel as a movable position heating source under remote control. *Small*, 10(14), 2796–2800. <https://doi.org/10.1002/sml.201400477>